A Near-Wall Reynolds Stress Model for Backward-Facing Step Flows

Sungho Ko*

(*Received July 10, 1998*)

A near-wall Reynolds stress model has been used in numerical computations for two-dimensional, incompressible turbulent flows over backward-facing steps. Numerical results are compared with Direct Numerical Simulation data as well as experimental data for flow quantities such as the skin friction, wall pressure, U-velocity and the Reynolds stress. Budgets of the transport equations for the U-velocity, turbulence kinetic energy, k and the Reynolds shear stress, $-\overline{uv}$ are also calculated and compared with the Direct Numerical Simulation data. The comparison reveals that the near-wall Reynolds stress model predicts the reattachment length fairly accurately. The near-wall Reynolds stress model also predicts the development of the boundary layer downstream of the reattachment point correctly when the Reynolds number is low. However, the model generally predicts a weak separation bubble and a slowly developing boundary layer when the Reynolds number is high.

Key Words: Backward-Facing Step, Reynolds Stress Model, Near-Wall, Turbulent Flow, Turbulence Model, Finite Volume, SIMPLER

1. Introduction

Separation and reattachment of turbulent shear layers are observed in many important engineering applications, yet are poorly understood. This has motivated many studies on understanding and predicting the processes of separation and reattachment of turbulent shear layers. Whether the separated/reattached turbulent flows are induced by the adverse pressure gradient or by discontinuities of geometry, the complex flow phenomena have attracted special attention of turbulence model developers. It is still a formidable task for the model developers to formulate the turbulence closure models to predict the essential features of separated turbulent flows accurately.

For the past two decades, the backward-facing step flow, which is the simplest separated flow, has been a popular test case for turbulence models. Although detailed studies on the performance of many turbulence models for flows over backward-facing steps can be found in a large number of papers, only the few papers that are closely related to the study are listed.

Yoo *et al.* (1989) calculated a backward-facing step flow using the Reynolds stress model proposed by Launder *et al.* (1975). They found that the Reynolds stress models predicted the flow field better than a standard k-ε model in the recirculating region. They also noticed that the recovery rate of the redeveloping boundary layer downstream of the reattachment point is too slow. Park *et al.* (1992) applied a standard k-ε model and a non-linear k-ε model to three-dimensional backward-facing step flow. They found that the reattachment length of the three-dimensional flow was considerably shorter than the corresponding two-dimensional flow. Thangam & Speziale (1992) and Lasher & Taulbe (1992) reported extensive literature survey and numerical investigation for the backward-facing step flows. These studies indicate that almost all the existing turbulence models fail to predict many important features of the backward-facing step flow accurately, such as the reattachment length, recovery

* Department of Mechanical Design Engineering, Chungnam University, Taejon 305-764, Korea

rate of the redeveloping boundary layers downstream of the reattachment point, streamlines near the reattachment point, and the skin friction coefficient.

An elliptic relaxation model was proposed by Durbin (1991) to represent inhomogeneous effects of wall-bounded shear flows near the surface. This model obviated the need for ad hoc eddy viscosity damping functions in the near wall region. After showing that the elliptic relaxation approach was successful in simple flows, such as the channel flow and flat plate, and the attached boundary layers, the model was extended to a full near-wall Reynolds stress model (Durbin, 1993) (herein after NRSM).

Using the NRSM, Ko & Durbin (1993) computed the massively separated boundary layer experiment of Simpson *et al.* (1981), and found that the new model was able to produce a separated flow reasonably. However, it was difficult to draw any conclusion on the model performance due to ambiguities in the experimented flow condition. Therefore, it is necessary to have a well-defined test case with clear-cut boundary conditions in order to isolate the phenomena which are directly related to the turbulence model. In addition, the Direct Numerical Simulation (herein after DNS) data (Le *et al.*, 1997) has become available for detailed comparison for a low Reynolds number backward-facing step flow.

The main objectives of the present study are to apply the NRSM to the flows over backward-facing steps, and to test the validity of the model by comparing with the newest DNS data.

2. Turbulence Model

As discussed previously, the NRSM is capable of describing near-wall effects without using *ad hoc* damping functions. The model utilizes the elliptic differential equations to account for non-local wall blocking effects. Here, only the model equations are briefly described. Detailed discussion of the model and its boundary conditions can be found in papers by Durbin (1991, 1993).

For a Newtonian fluid with the uniform-density, uniform-viscosity, and no external force, the Reynolds stress transport equation is given as

$$\frac{D\overline{u_iu_j}}{Dt}=P_{ij}-\frac{1}{\rho}\left(u_i\frac{\partial p}{\partial x_j}+u_j\frac{\partial p}{\partial x_i}\right)-\varepsilon_{ij}+\frac{\partial}{\partial x_m}\left[\nu\frac{\partial\overline{u_iu_j}}{\partial x_m}-\overline{u_mu_iu_j}\right] \quad (1)$$

where

$$P_{ij}=-\left(\overline{u_iu_k}\frac{\partial U_j}{\partial x_k}+\overline{u_ju_k}\frac{\partial U_i}{\partial x_k}\right) \quad (2)$$

is the rate of turbulence production by mean velocity gradients. This production rate does not introduce further unknowns and thus does not require modeling. The triple velocity correlation in Eq. (1), representing the rate at which the Reynolds stress is carried by the turbulence fluctuations, is modeled by the simple gradient-diffusion hypothesis of Daly & Harlow (1970):

$$\frac{\partial}{\partial x_m}\left(-\overline{u_mu_iu_j}\right)=\frac{\partial}{\partial x_m}\left(\frac{\nu_{mt}}{\sigma_k}\frac{\partial\overline{u_iu_j}}{\partial x_l}\right) \quad (3)$$

The tensorial eddy viscosity in Eq. (3) is

$$\nu_{mt}=C_\mu\,\overline{u_mu_l}\,T \quad (4)$$

where the Lagrangian time-scale, T, of the turbulence is

$$T=\max\left(\frac{k}{\varepsilon},\ C_T\sqrt{\frac{\nu}{\varepsilon}}\right) \quad (5)$$

The second term in (5) introduces the Kolmogoroff time-scale as a lower bound. The rest of the unclosed terms, such as pressure gradient-velocity correlations and anisotropic dissipation, ε_{ij} are lumped into a term, F_{ij} as

$$F_{ij}=-\frac{1}{\rho}\left(u_i\frac{\partial p}{\partial x_j}+u_j\frac{\partial p}{\partial x_i}\right)-\varepsilon_{ij}+\frac{\overline{u_iu_j}}{k}\varepsilon \quad (6)$$

By combining Eq. (3) through Eq. (6), Eq. (1) becomes

$$\frac{D\overline{u_iu_j}}{Dt}=P_{ij}+F_{ij}-\frac{\overline{u_iu_j}}{k}\varepsilon+\frac{\partial}{\partial x_m}\left[\left(\nu+\frac{\nu_{mt}}{\sigma_k}\right)\frac{\partial\overline{u_iu_j}}{\partial x_l}\right] \quad (7)$$

In Eq. (7), F_{ij} is the only unclosed term, which can be modeled using the elliptic relaxation model (Durbin, 1993) as follows

$$F_{ij}=kf_{ij} \text{ and} \quad (8)$$

$$L^2\nabla^2f_{ij}-f_{ij}=\frac{C_1}{T}\left(\frac{\overline{u_iu_j}}{k}-\frac{2}{3}\delta_{ij}\right)+\frac{C_2}{k}\left(P_{ij}-\frac{2}{3}P\delta_{ij}\right) \quad (9)$$

where the length-scale L in Eq. (9) is expressed as

$$L=C_L \max\left(\frac{k^{3/2}}{\varepsilon},\ C_\eta\left(\frac{\nu^3}{\varepsilon}\right)^{1/4}\right) \tag{10}$$

and $P=P_{ii}/2$.

The elliptic relaxation model represents kinematic blocking of the wall (Hunt and Graham 1978) by elliptic differential Eq. (9). In incompressible flow, pressure fluctuations obey an elliptic equation (i. e. Poisson's equation), so it seems natural to introduce ellipticity into F_{ij} which represents pressure-velocity correlations. The right hand side of Eq. (9) is simply the 'basic' model of Launder *et al.* (1975). Any other quasi-homogeneous Reynolds stress model could be used as the source term in this equation. Thus, the elliptic relaxation formulation primarily provides a framework for extending a quasi-homogeneous model to a model for near-wall turbulence. The constants for the NRSM are $C_\mu=0.28$, $C_T=6.0$, $C_1=1.22$, $C_2=0.6$, $C_L=0.18$, and $C_\eta=80.0$.

The above NRSM equations are coupled with the transport equations for turbulent kinetic energy k and its rate of dissipation ε as

$$\frac{Dk}{Dt}=P-\varepsilon+\frac{\partial}{\partial x_m}\left\{\left(\nu+\frac{\nu_{ml}}{\sigma_k}\right)\frac{\partial k}{\partial x_l}\right\} \tag{11}$$

$$\frac{D\varepsilon}{Dt}=C_{\varepsilon 1}\left(1+0.1\frac{P}{\varepsilon}\right)\frac{P}{T}-C_{\varepsilon 2}\frac{\varepsilon}{T}+\frac{\partial}{\partial x_m}\left\{\left(\nu+\frac{\nu_{ml}}{\sigma_\varepsilon}\right)\frac{\partial \varepsilon}{\partial x_l}\right\} \tag{12}$$

The constants for the k-ε system of equations are $C_{\varepsilon 1}=1.44$, $C_{\varepsilon 2}=1.85$, $\sigma_k=1.0$, and $\sigma_\varepsilon=1.3$.

3. Numerical Method

The NRSM are implemented into a full Navier-Stokes solver for 2-D, incompressible, steady-state turbulent flows over the backward-facing step. This solver is based on the finite volume procedures embodied in the TEACH code of Gosman & Pun (1974). The equations of primitive variables are solved on a system of staggered grids using the SIMPLER algorithm of Patankar (1980). The third-order accurate QUICK differencing scheme of Leonard (1979) is utilized for all convective terms in the momentum equations to reduce the artificial viscosity.

The accuracy of the numerical prediction depends on the accuracy of the numerical methods used as well as on the ability of the turbulence model applied to a specific flow situation. Two-dimensional laminar flow over a backward-facing step has been computed in order to verify the accuracy of the numerical methods (Ko, 1995). This explanatory computation has shown that the present computational methods are adequate to be applied to the backward-facing step flow.

The computational domain is extended from the step ($x=0$) to 40 H, where H is step height. This long computational domain ensures that the zero-normal gradient boundary condition in the axial direction for all flow variables at the outlet, $\partial/\partial x=0$, is appropriate.

At the inlet boundary, profiles of all the flow variables are specified. The whole computation procedure and the resulting flowfield are sensitive to the specified inlet conditions since the inlet boundary at the step is the onset of sudden changes of flow parameters. In the present study, the inlet profiles of flow variables are obtained using the following procedures: (1) obtain the displacement thickness, δ^* and the Reynolds number, Re, based on the reference velocity U_o and the step height H at the step from experimental data, (2) calculate the mean U-velocity, U_m for the channel upstream of the step using the relation $U_m=U_o(1-2\delta^*_{in}/H_1)$, where H_1 is the channel height at the inlet, (3) run a channel calculation starting with a plug flow with the mean velocity, U_m at the inlet, (4) find the downstream location where the calculated displacement thickness δ^* coincides with δ^*_{in}, and (5) finally use the channel solution at that location for the inlet boundary conditions for the backward-facing step flow problems.

After exploratory runs, the selected grids are of 140 of uniformly expanding grid lines in the streamwise direction and 140 (107 for Jovic & Driver's (1994) case) with highly non-uniform grid lines in the transverse direction. The grid distribution is not made larger or smaller over the neighborhood more than 8 to 10% depending on

Table 1 Test cases for backward-facing step flows.

Group	$E_r=H_1/H_2$	$Re_h=U_oH/\nu$	δ^*/H	Meas. X_r	Pred. X_r
Kim *et al.*	1.5	45,000	0.0387	7	6.8
Driver and Seegmiller	1.125	37,500	0.2	6.3	6.1
Jovic and Driver	1.2	5,000	0.19	6	5.4
Le, Moin and Kim	1.2	5,000	0.19	6	-

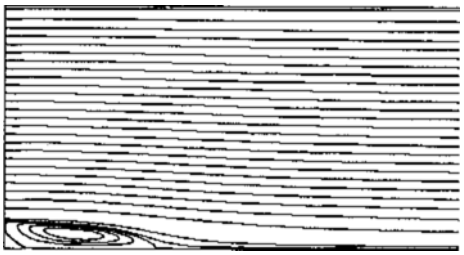

Fig. 1 Computed streamlines for Driver and Seegmiller case.

the test cases. The first grid point off the wall is at $y^+ \leq 0.5$, where the wall unit y^+ is defined as $y^+ \equiv yu_\tau/\nu$, $u_c=\sqrt{\tau_w/\rho}$ and τ_w is the wall shear stress.

4. Results and Discussion

Computations of turbulent backward-facing step flows are done using the NRSM for the same flow conditions as experiments of Kim *et al.* (1980) (KKJ), Driver and Seegmiller (1985) (DS), and Jovic & Driver (1994) (JD). DNS data of Le *et al.* (1997) (LMK) are used for detailed comparison of the Reynolds-stress budgets.

Table 1 summarizes the flow conditions of the test cases. H_1 is the channel height at the inlet, H_2 is the channel height at the outlet and H is the step height. Note that it is desirable to have a small expansion ratio E_r to minimize free stream pressure gradient effects (Badri Narayanan *et al.*, 1974). The KKJ case is subjected to significant free stream pressure gradient effects due to the large expansion ratio whereas the other two cases are not. Notice also that JD's experiment and LMK's DNS have identical flow conditions; in fact, JD's experiment was performed in order to verify the accuracy of the DNS. The predicted reattachment lengths X_r for all cases are in very good agreement with the measured X_r, although slightly underestimated.

Figure 1 shows the calculated streamlines for DS case (with zero deflection angle of the top wall). The sharp discontinuity of the backward-facing step geometry produces a strong shear layer near the step. A large recirculation region is formed underneath of the shear layer, which, in turn, creates a small eddy motion in the corner. As the shear layer spreads, it impinges on the bottom wall near the reattachment point X_r. Some of the impinging shear layer moves downstream and starts to develop into a boundary layer (the redeveloping boundary layer). Notice that the present streamline profiles do not show an unrealistic behavior of the separation streamline near the reattachment point. Lasher and Taulbee (1992) observed that the separation streamline was pulled back underneath the recirculating region when a fine grid was used in the near-wall region. In the present study, a fine grid was used and that spurious behavior was observed.

Figure 2(a), 2(b) and 2(c) show calculated skin friction coefficients C_f for JD, DS and KKJ cases, and results are compared with the corresponding experimental and DNS data. In all three cases, the model calculations underpredict the negative peak values of C_f in the recirculation zones. Also, for DS and KKJ cases (Figs. 2(b) and 2(c)), the calculated C_f is significantly lower than the experimental data in the regions downstream of X_r, which means slow and weak recovery of the redeveloping boundary layer. It is interesting to note that, for JD's low Reynolds number case (Fig. 2(a)), the negative peak of the measured C_f in the recirculation region is compa-

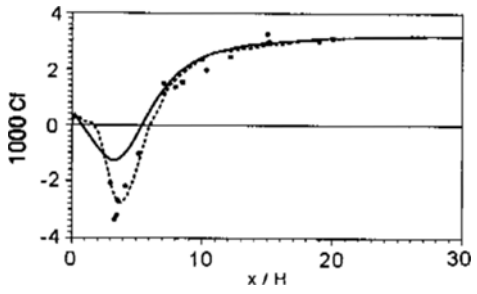

(a) Jovic and Driver case

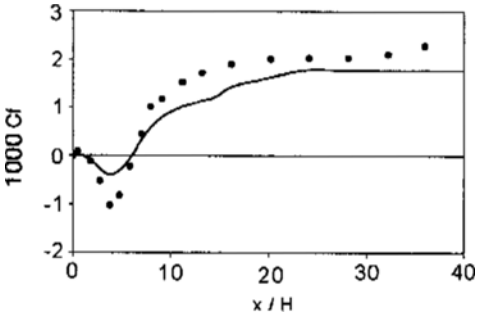

(b) Driver and Seegmiller case

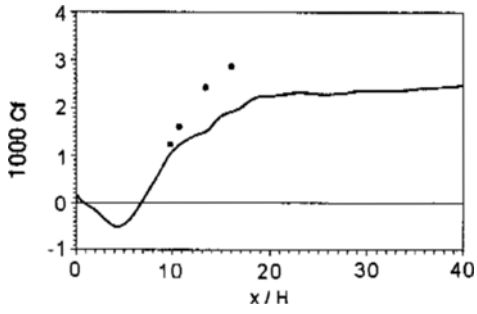

(c) Kim *et al.* case

Fig. 2 Profiles of skin friction coefficients: ——, NRSM; ----, DNS; ●, experimental data.

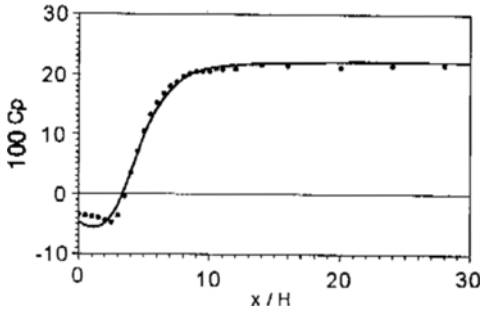

(a) Jovic and Driver case: ——, NRSM; ----, DNS; •, experimental data.

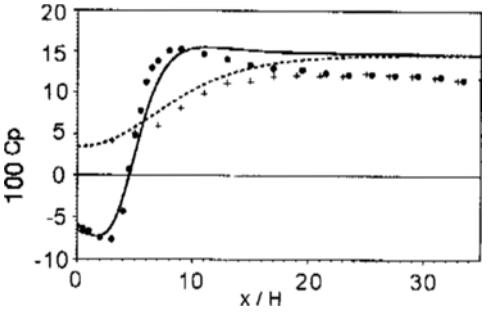

(b) Driver and Seegmiller case: ——, NRSM, •, experimental data., step-wall; ----, NRSM, |, experimental data, opposite-wall.

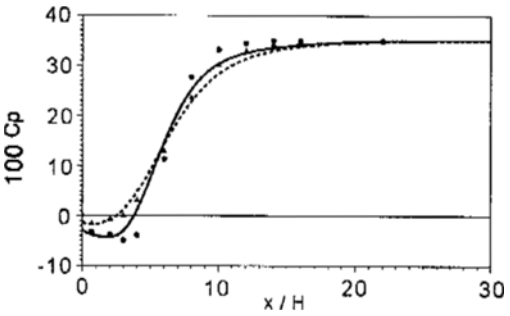

(c) Kim *et al.* case: ——, NRSM, •, experimental data., step-wall; ----, NRSM, ▲ experimental data, opposite-wall.

Fig. 3 Profiles of surface pressure coefficients.

rable in magnitude to that in the redeveloping boundary layer region downstream of the reattachment point.

Surface pressure coefficients $C_p(\equiv 2(P-P_o)/(\rho U_o^2))$ are shown in Figs. 3(a), 3(b) and 3(c) for JD, DS and KKJ cases. The calculations show fairly good agreement with the measurements for the JD and DS cases with minor deviation. The agreement for the KKJ case (Fig. 3(c)) is relatively poor.

Figure 4(a), 4(b) and 4(c) show the streamwise mean velocity profiles at various positions upstream and downstream of the reattachment point, and results are compared with the experimental data of JD, DS and KKJ. In general, the agreement of the computational results with the experimental data is very good. For JD case (Fig. 4(a)), the computed U-velocity profiles at $x/H=4$ shows insufficient backflow in the recirculation region. However, the model computation

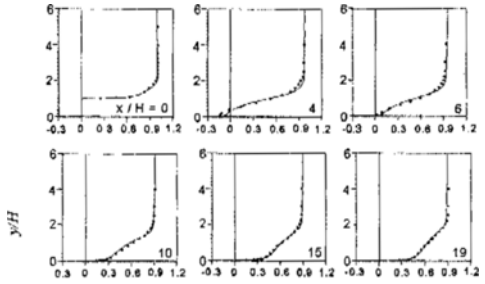

(a) Jovic and Driver case

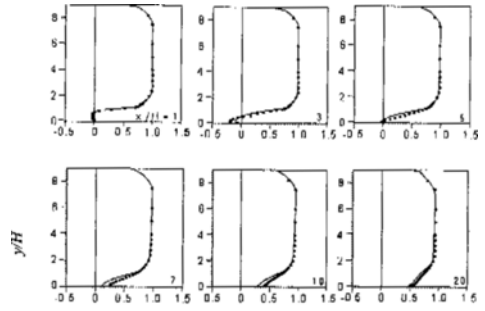

(b) Driver and Seegmiller case

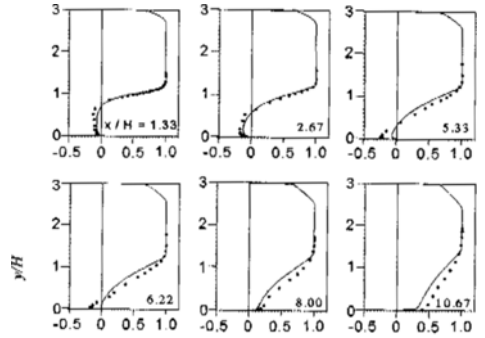

(c) Kim *et al.* case

Fig. 4 Mean U-velocity profiles: ——, NRSM; ●, experimental data.

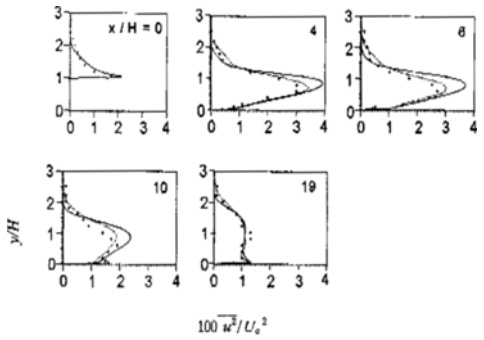

(a) $\overline{u^2}$

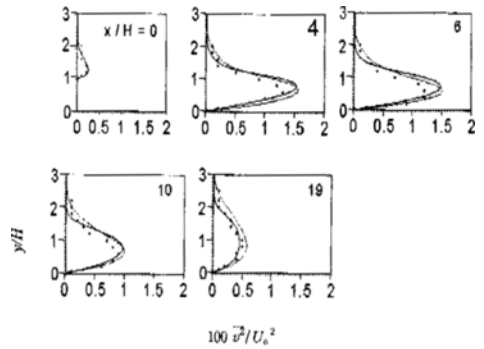

(b) $\overline{v^2}$

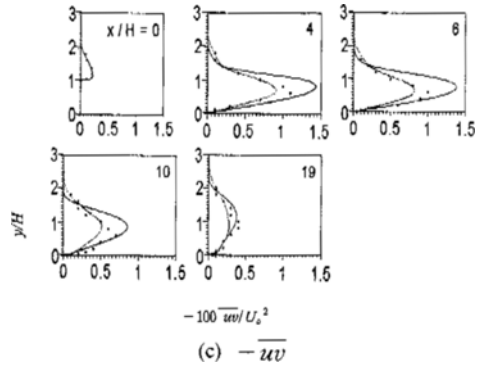

(c) $-\overline{uv}$

Fig. 5 Reynolds stress profiles for Jovic and Driver case: ——, NRSM; ----, DNS; ●, experiemental data.

predicts the redeveloping boundary layer almost perfectly for JD's low Reynolds number case. For higher Reynolds number cases, DS and KKJ cases, the computations predict not only weak separated regions but also slow recovery of the redeveloping boundary layers downstream of X_r. This finding suggests that the DNS data for low Reynolds number flows might not be suitable for developing turbulence models that are mainly used for high Reynolds number flows.

Figure 5(a), 5(b) and 5(c) show the comparison of computed profiles of the Reynolds stress components $\overline{u}^2$, $\overline{v}^2$, and $-\overline{uv}$ at various positions upstream and downstream of the reattachment point with the JD's experimental data and LMK's DNS data. It is quite encouraging to see that all

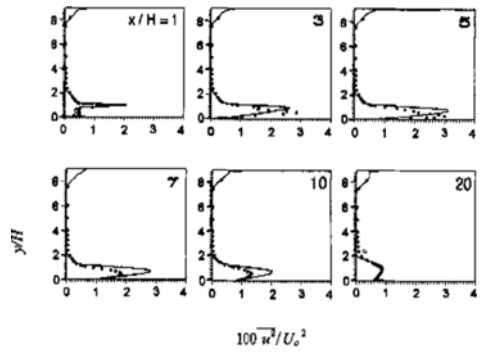

(a) $\overline{u^2}$

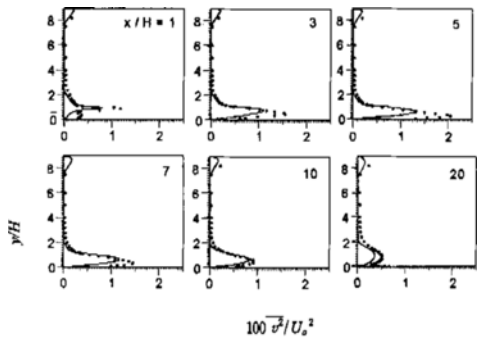

(b) $\overline{v^2}$

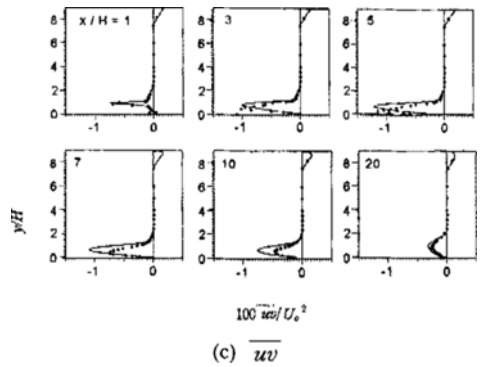

(c) $\overline{uv}$

Fig. 6 Reynolds stress profiles for Driver and Seegmiller case: ——, NRSM; ●, experimental data.

three Reynolds stress profiles at the step of this study, which are obtained from the channel flow solution with the same values of Re and δ^* as those of the experiment, show excellent agreement with the experimental data. Thus the inlet boundary conditions are in accord with the experiment. In Fig. 5(a), the $\overline{u^2}$ profiles at $x/H=4$ and 6 represent the dominance of the shear layer. At $x/H=10$, JD's experimental data already show double peaks of the $\overline{u^2}$ profile , one peak being very near the wall, while the DNS as well as the computation results of this study are slowly catching up this development, as shown in the profiles at $x/H=19$. In addition, the $\overline{u^2}$ profiles at $x/H=19$ indicate that the redeveloping boundary layer is not fully recovered from the free shear layer. In the region of $x/H\leq 10$, the maximum values of $\overline{u^2}$ are overpredicted by the present computation. The agreement between the calculated and the measured $\overline{v^2}$ profiles in Fig. 5(b) is as good as the agreement between the DNS data and the measurements. In Fig. 5(c), the model calculations overpredicts the peak values of $-\overline{uv}$ in the region near the reattachment point, while the DNS underpredicts.

The calculated Reynolds stress components $\overline{u^2}$, $\overline{v^2}$, and $\overline{uv}$ are compared with the DS's experimental data as shown in Figs. 6(a), 6(b) and 6(c). As observed in these figures, the profiles of the Reynolds stresses in the region near the top wall remain relatively unchanged, which indicates the minimal freestream pressure gradient effects due to the step. In Fig. 6(a), the calculated $\overline{u^2}$ profiles at $x/H=7$ and 10 show the peaks overpredicted by nearly 50%. In the recirculation region, the calculations show the peaks located higher than the experimental data. In Fig. 6(b), the calculation underpredicts the peaks of $\overline{v^2}$ and the slope of $\overline{v^2}$ in y-direction in the near-wall region. In the $\overline{uv}$ profiles in Fig. 6(c), the discrepancies are almost the same as in the $\overline{u^2}$ profiles in Fig. 6(a).

Figures 7, 8 and 9 compare the calculated budgets of the transport equations of U-velocity, k and $\overline{uv}$ with LMK's DNS data at four different positions upstream and downstream of the reattachment point. Lines represent the model calculation and the symbols are the DNS data. Note that all terms in the k-equation are normalized by the reference velocity U_o and the step height H, multiplied by 100.

In Fig. 7, the convection term $-U_k\partial U/\partial x_k$ is balanced by the sum of the Reynolds stress gradient $\partial(-\overline{uu_k})/\partial x_k$ and the pressure gradient

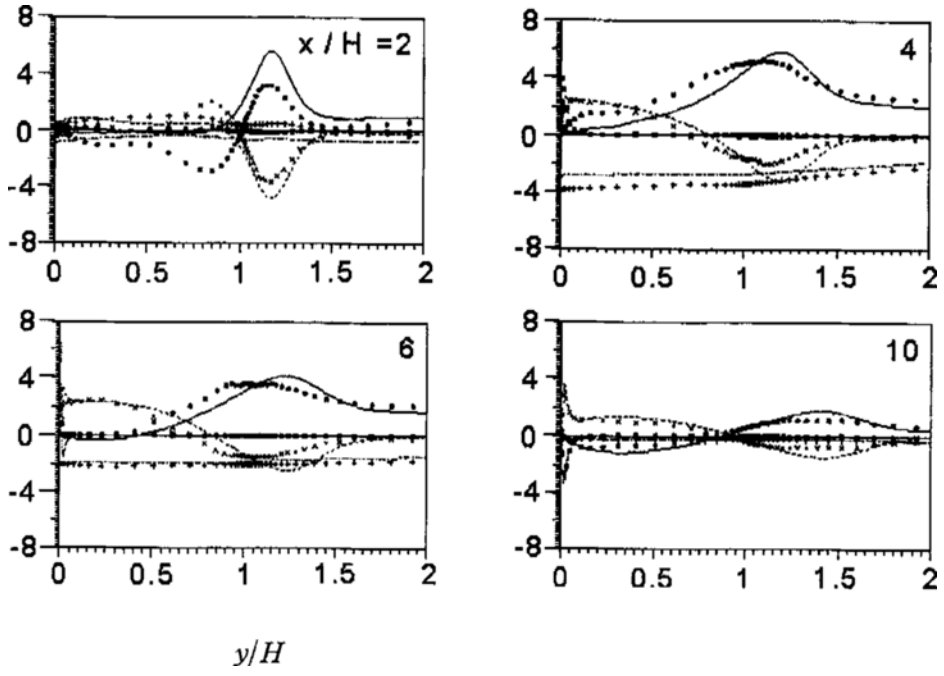

Fig. 7 Budgets of the mean U-momentum equation for Jovis and Driver case (lines are NRSM prediction and symbols are DNS data) :
——, ●, $-U_k\partial U/\partial x_k$; ——, +, $-\partial P/\partial x$;---, X, $\partial(-\overline{uu_k})/\partial x_k$; ---, ■, $\nu\partial/\partial x_k(\partial U/\partial x_k)$.

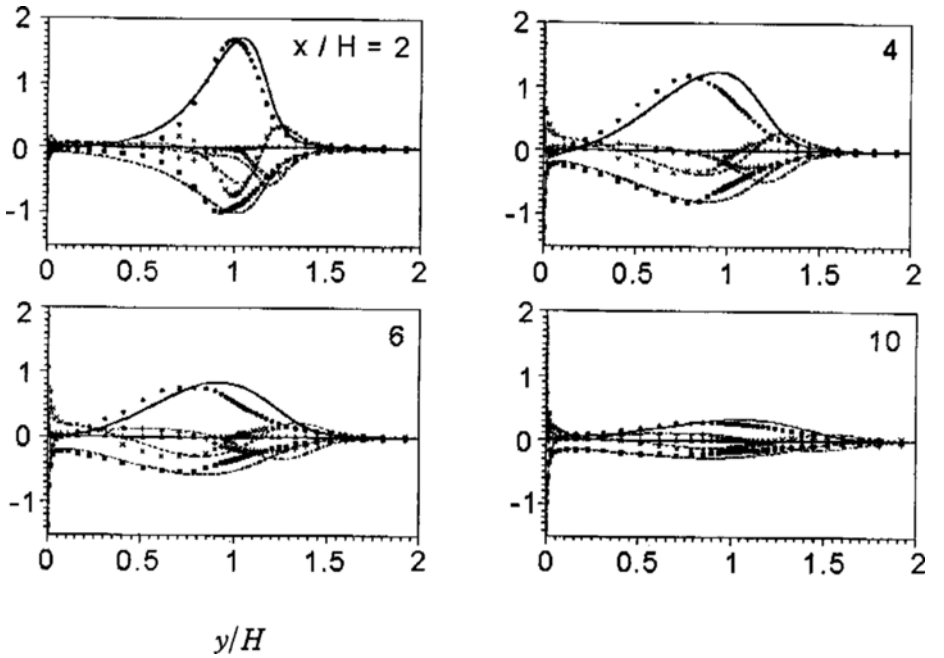

Fig. 8 Budgets of the k-equation for Jovic and Driver case (lines are NRSM prediction and symbols are DNS data) :
——, +, $-U_m\partial k/\partial x_m$; ——, ●, P; ——, ■, ε; ---, Δ, $\partial/\partial x_m\{\nu/\sigma_k(\partial k/\partial x_m)\}$;
---, X, $\partial/\partial x_m\{\nu_m/\sigma_k(\partial k/\partial x_l)\}$.

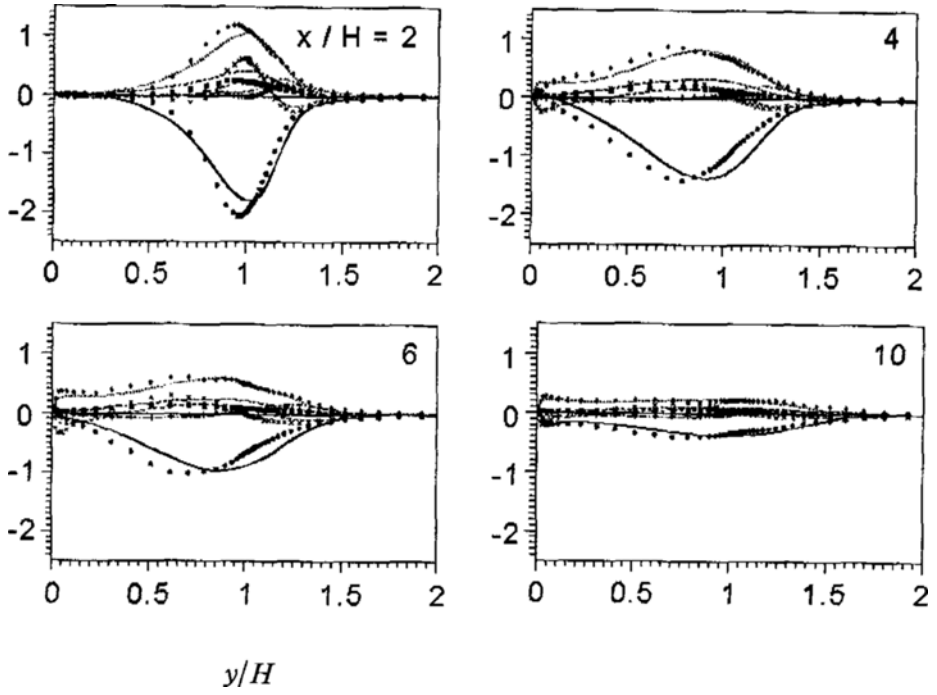

Fig. 9 Budgets of the $\overline{uv}$-equation for Jovic and Driver case (lines are NRSM prediction and symbols are DNS data): ——, +, $-U_m\partial\overline{uv}/\partial x_m$; ——, ●, P_{12}; ---, ◇, F_{12}; ---, X, $\partial/\partial x_m\{\nu_{ml}/\sigma_k(\partial\overline{uv}/\partial x_l)\}$; ——, ■, $(\overline{uv}/k)\varepsilon$.

$-\partial P/\partial x$. Since the Reynolds stress gradient is the only term through which the turbulence acts on the mean momentum, it is quite important to understand the meaning of the profiles of $\partial(-\overline{uu_k})/\partial x_k$. The major deviation in the $\partial(-\overline{uu_k})/\partial x_k$ profiles is found in the negative peak levels. The viscous diffusion terms, $\nu\partial/\partial x_k(\partial U/\partial x_k)$ are negligible compared to other terms everywhere except in the region very near the wall. Notice that at $x/H=2$, the calculation shows negative $-\partial P/\partial x$ while the DNS data positive. This deviation seems to be resulted from the deviation in the convection terms. Considering that the pressure is elliptic in nature, it is possible that the deviation in $-\partial P/\partial x$ comes from the present computational inlet located right at the step. This problem may go away if the inlet of the computational domain is located a few step-heights upstream of the step. Moving downstream, the agreement between the model computation and the DNS data becomes better. In fact, the agreement is very good at $x/H=10$ where the $-\partial P/\partial x$ term is negligible.

As shown in Fig. 8, the production rate P in the transport equation of the turbulence kinetic energy k is balanced mainly by the sum of the dissipation rate ε, the convection $-U_m\partial k/\partial x_m$ and the turbulent diffusion $\partial/\partial x_m\{\nu_m/\sigma_k(\partial k/\partial x_l)\}$. The viscous diffusion $\partial/\partial x_m\{\nu/(\partial k/\partial x_l)\}$ is negligible everywhere. Notice from the profiles of the turbulent diffusion that the turbulence kinetic energy is extracted from the middle of the shear layer and then transferred to the outer regions of the shear layer. Overall, the model calculation shows very good agreement with the DNS data.

In the budget of the $\overline{uv}$ transport equation in Fig. 9, the production rate P_{12} is balanced by the sum of the redistribution F_{12} and the turbulent diffusion, according to the DNS data. However, the present calculation shows that the contribution from the turbulent diffusion is somewhat smaller than that from the anisotropic dissipation.

5. Concluding Remarks

A near-wall Reynolds stress model(NRSM) was used in numerical computations for two-dimensional, incompressible turbulent flows over backward-facing steps. Numerical results for three different backward-facing step flows were compared with the DNS data as well as the experimental data. The comparison revealed that the NRSM predicted the reattachment length fairly accurately. The NRSM also fairly well predicted the development of the boundary layer downstream of the reattachment point correctly when the Reynolds number was low. However, the model generally predicted a weak separation bubble and a slowly developing boundary layer when the Reynolds number was high.

In order to scrutinize the model, the calculated budgets of the transport equations of U-velocity, k and $\overline{uv}$ were compared with DNS data at four different positions upstream and downstream of the reattachment point. Overall, the model calculation showed very good agreement with the DNS data.

References

Badri Narayanan, M. A., Khadgi, Y. N. and Viswanath, P. R., 1974, "Similarities in Pressure Distribution in Separated Flow Behind Backward-Facing Steps," *The Aeronautical Quarterly*, Vol. 25, pp. 305~312.

Daly, B. J. and harlow, F. H., 1970, "Transport Equations of Turbulence," *Phys. Fluids*, Vol. 13, pp. 2634~2649.

Driver, D. and Seegmiller, H. L., 1985, "Features of a Reattaching Turbulent Shear Layer in Divergent Channel Flow," *AIAA J.*, Vol. 23, pp. 163~171.

Durbin, P. A., 1991, "Near-Wall Turbulence Closure Modeling Without 'Damping Functions'," *Theoretical and Computational Fluid Dynamics*, Vol. 3, pp. 1~13.

Durbin, P. A., 1993, "A Reynolds Stress Model for Near-Wall Turbulence," *J. Fluid Mech.*, Vol. 249, pp. 465~498.

Gosman, A. D. and Pun, W. M., 1974, "Calculations of Recirculating Flows," Research Report No. HTS/74/2., Dept. Mech. Engr., Imperial College, London, England.

Jovic, S. and Driver, D., 1994, "Backward-Facing Step Measurements at Low Reynolds Number," NASA TM 108807.

Kim, J., Kline, S. J. and Johnston, J. P., 1980, "Investigation of a Reattaching Turbulent Shear Layer: Flow over a Backward-Facing Step," *J. Fluids Engr.*, Vol. 102, pp. 302~308.

Ko, S., 1995, "Comparison of Finite Differencing Schemes for Laminar Flows over Backward-Facing Step," *Proceedings of the 3rd CFD workshop of KSME*, pp. 169~171.

Ko, S. and Durbin, P. A., 1993, "Application of a Near-Wall Turbulence Model to Adverse Pressure Gradient and Separating Boundary Layers," *Near-Wall Turbulent Flows*, edited by So et al., Elsevier, pp. 145~153.

Lasher, W. C. and Taulbee, D. B., 1992, "On the Computation of Turbulent Backstep Flow," *Int. J. Heat and Fluid Flow*, Vol. 13, pp. 30~40.

Launder, B. E., Reece, G. J. and Rodi, W., 1975, "Progress in the Development of a Reynolds-Stress Turbulence Closure," *J. Fluid Mech.*, Vol. 68, pp. 537~566.

Le, H. and Moin, P., and Kim, J, 1997, "Direct Numerical Simulation of Turbulent Flow over a Backward-Facing Step," *J. Fluid Mech.*, Vol. 330, pp. 349~374.

Leonard, B. P., 1979, "A Stable and Accurate Convective Modelling Procedure Based on Quadratic Upstream Interpolation," *Computer Methods in Applied Mechanics and Engr.*, Vol. 19, pp. 59~98.

Park, S. O., Lim, K. S. and Pletcher, R. H., "A Numerical Study of Three-Dimensional Backward-Facing Step Flow," *KSME J.*, Vol. 7, pp. 1~13.

Patankar, S. V., 1980, *Numerical Heat Transfer and Fluid Flow*, McGraw-Hill, New York.

Simpson, R. L., Chew, Y. -T., and Shivaprasad, B. G., 1981, "The Structure of a Separating Turbulent Boundary Layer. Part 1. Mean Flow and Reynolds Stresses," *J. Fluid Mech.*, Vol. 113, pp. 23~51.

Thangam, S. and Speziale, C. G., 1992, "Turbulent Flow Past a Backward-Facing Step: A Critical Evaluation of Two-Equation Models," *AIAA J.*, Vol. 30, pp. 1314~1320.

Yoo, J. Y., Choi, H. C. and Han, S. M., 1989, "Numerical Analysis of Turbulent Flow over a Backward-Facing Step Using Reynolds Stress Closure Model," *KSME J.*, Vol. 3, pp. 31~37.